Nanotechnology **18** (2007) 285501 (7pp) doi:10.1088/0957-4484/18/28/285501

Gas sensing behaviour of mat-like networked tungsten oxide nanowire thin films

B Deb[1], S Desai[2], G U Sumanasekera[2,3] and M K Sunkara[1,4]

[1] Department of Chemical Engineering, University of Louisville, KY 40292, USA
[2] Department of Electrical Engineering, University of Louisville, KY 40292, USA
[3] Department of Physics, University of Louisville, KY 40292, USA

E-mail: mahendra@louisville.edu

Received 11 April 2007, in final form 16 May 2007
Published 15 June 2007
Online at stacks.iop.org/Nano/18/285501

Abstract

Here, we present the results of the resistive response of tungsten trioxide nanowire (mat-like, nanowire networks) and nanoparticle thin films subjected to N_2O gas in the temperature range of 373–773 K. The nanowire mats exhibited an order of magnitude higher response in the resistivity change compared to that of nanoparticle films at temperatures above 523 K. Nanowire mats also exhibited relatively faster adsorption and desorption times. Impedance spectroscopy studies showed that the gas sensing mechanism for nanowire mats involves changes in both the nanowire and grain boundary resistances, whereas for nanoparticle films only the grain boundary resistance governs the sensor properties upon exposure to gases.

1. Introduction

Recently, the nanocrystalline metal oxide materials have attracted interest for gas sensing applications due to their increased surface-to-volume ratio and high density of surface sites [1–8]. The thin film sensors usually work by changing the surface conductivity of the active material due to the surface adsorption of the gas species and related space charge effects. Therefore, the gas detection ability dramatically increases with decreasing grain size [9] and the surface-to-volume ratio limits the maximum sensitivity [10]. Porous thin films were often preferred to overcome this problem because they offer increased surface-to-volume ratios [11, 12].

Single nanowire devices and nanowire arrays offer great potential for high sensitivity with their ultrahigh surface-to-volume ratio. These devices are just beginning to be explored. For example, single nanowire devices using SnO_2, TiO_2, ZnO, In_2O_3 and WO_3 nanowires have been fabricated and their performances have been investigated in terms of operating temperature, sensitivity and response time [13–23]. In the case of single nanowire devices, an excellent review [24] proposed that a small change in the chemical state of the surface can cause depletion/accumulation of electron/holes not only near the surface but also in the entire volume of the nanostructure. The fast response and recovery times of these types of device depend on ultra fast adsorption/desorption kinetics between the nanowire surface and the gas phase. Recent reports of ethanol vapour detection by $ZnSnO_3$ nanowires show the response and recovery time to be as fast as 1 s [25]. However, the fabrication of single nanowire devices and parallel nanowire array devices require cumbersome post-growth processing [8, 14, 19, 26, 27].

On the other hand, thin films containing nanowires in a highly networked fashion could probably be used for making gas sensing devices with behaviour similar to that of single nanowire devices without much post-processing effort. This is possible only when the individual nanowires within the mat are covalently bonded to each other and the mat closely resembles that of two- and three-dimensional networks of nanowires. In a recent paper, synthesis of a nanowire thin film containing branched tungsten oxide nanowires was reported that simulated a type of three-dimensional nanowire network [28]. The sensors made using such films yielded promising gas detection performances.

In our study, we deposited mat-like three-dimensional networks of nanowire films and investigated their gas sensing behaviour and compared it to that of the nanoparticle thin films. Trace amounts of nitrous oxide (N_2O) diluted in nitrogen were

[4] Author to whom any correspondence should be addressed.

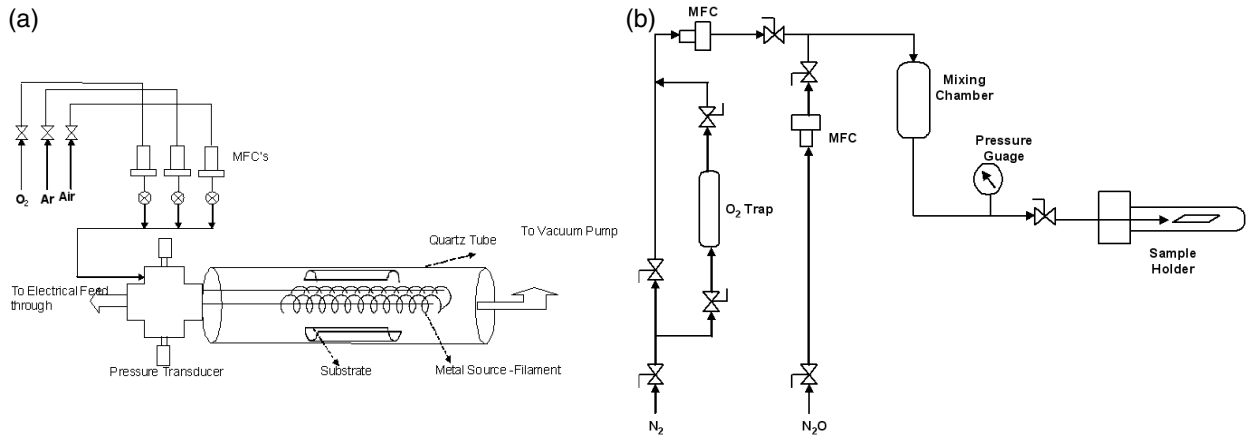

Figure 1. (a) A schematic diagram of the hot-filament chemical vapour deposition (HFCVD) reactor used for synthesizing nanowire mats and nanoparticle thin films and (b) a schematic diagram of the experimental set-up used for gas sensing studies.

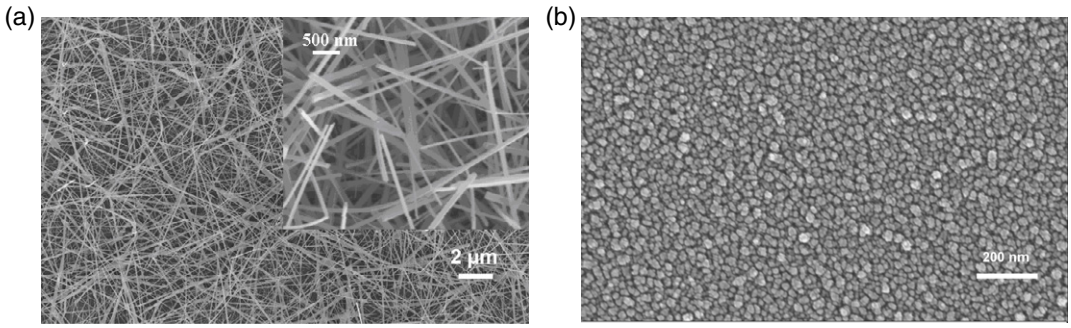

Figure 2. Scanning electron micrographs of (a) nanowire mat (the inset shows a high magnification image of the nanowire joints) and (b) nanoparticle samples.

used for determining the gas sensing performance of both types of sensors.

2. Experimental details

The WO_3 nanowire mats and nanoparticle films were deposited on quartz substrates using a custom-built, hot-filament chemical vapour deposition (HF-CVD) reactor shown in figure 1(a). The synthesis concept involves the generation of tungsten oxide species from tungsten filaments using oxygen and depositing tungsten oxide nanowires [29] and tungsten oxide nanoparticle thin films on quartz substrates.

As shown in figure 1(a), the HFCVD reactor is a 32 inch long, 2 inch diameter quartz tube located inside a tube furnace. The tungsten filament (99.95% purity, 0.5 mm diameter) wound over a boron nitride (BN) rod served as the metal source. The filament temperature and the oven temperature were maintained at 1700 °C and 800 °C, respectively. The pressure was maintained at 200 mTorr with a 100 sccm flow of argon and a 0.4 sccm flow of air. The temperature was high (>800 °C) owing to the radiation from the filament yielding low nucleation density on the substrate. Owing to the high synthesis temperature and low nucleation densities, the nanowires tend to grow parallel to the substrate making thin film containing 3D connections of nanowires. Lowering the temperature resulted in a higher nucleation density and randomly oriented nanowires forming dense thin films instead of the networks of nanowires [29]. Nanoparticle films were also obtained using the same set-up but at a chamber pressure of 300 mTorr using a 100 sccm flow of argon and a 0.2 sccm flow of oxygen. Nanowire mats and nanoparticle thin films were initially deposited onto 50 cm^2 quartz substrates and later cut into small pieces for fabricating gas sensors.

The gas sensing measurements were performed using a specially designed set-up as shown in figure 1(b). Two chromel/alumel thermocouples and two additional copper leads (0.003 inch diameter wires) were attached with small amounts of silver epoxy to the four corners of the 5 mm × 5 mm square sample. The apparatus was equipped with a turbo molecular pump capable of evacuating to 10^{-7} Torr for *in situ* studies in the temperature range of 77–600 K using a tube furnace and liquid nitrogen. The test gas was diluted with N_2 gas to give concentrations ranging from 1–100 ppm. The four probe resistance was measured using a constant current source (Keithley 2400) and a nano-voltmeter (Keithley 2182). Impedance measurements of the sensors at different temperatures were acquired using a potentiostat/galvanostat (EG&G 273 A) in the frequency range of 10 mHz–100 KHz.

3. Results and discussion

Figures 2(a) and (b) show SEM images of the nanowire mat and nanoparticle thin film samples. As shown in figure 2(a), the mat contains nanowires that are several microns

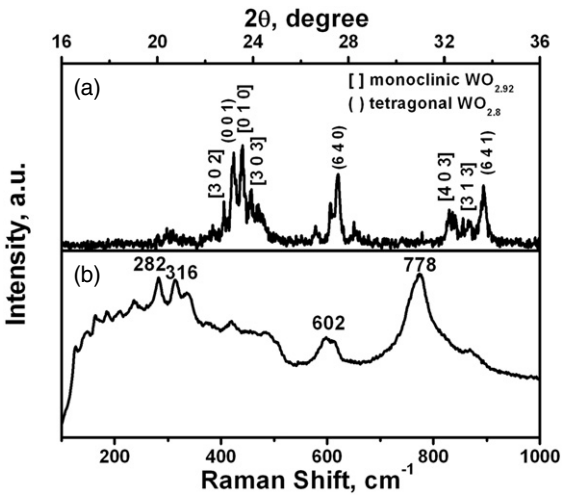

Figure 3. (a) Room temperature XRD spectrum of the nanowire mat sample showing the presence of both monoclinic and tetragonal phases and (b) room temperature Raman spectrum of the nanowire mat sample.

long and are bonded with several other nanowires forming three-dimensional nanowire networks. This type of mat-like morphology is different to that of a typical randomly oriented nanowire thin film (example: figure 5(a)) where each nanowire is randomly oriented and separated from the others. The x-ray diffraction patterns shown in figure 3(a) indicate that as-synthesized nanowires are made of oxygen deficient WO_3 phases. The presence of a mixture of monoclinic $WO_{2.9}$ and tetragonal $WO_{2.8}$ phases is evident and consistent with earlier observations [22–26].

The room temperature Raman spectra shown in figure 3(b) indicate crystalline phases of WO_3 within three main spectral regions between (i) 900–600 cm^{-1}, (ii) 400–200 cm^{-1} and (iii) below 200 cm^{-1}. It has been established that they correspond, respectively, to stretching, bending and lattice modes [30]. The Raman spectra for the nanowire sample showed two prominent peaks corresponding to the O–W–O stretching mode at 778 and 602 cm^{-1} which were shifted from the 809 and 714 cm^{-1} nanoparticle thin film values—not shown here—presumably due to oxygen deficiency in the nanowires. The absence of the 947 cm^{-1} peak in nanowire spectra indicates that there are no tungsten oxide hydrates ($WO_3 \cdot nH_2O$) present in the sample.

Typical sensor responses of both nanoparticle thin film and nanowire mat samples at 673 K are shown in figures 4(a) and (b). The samples were heated in vacuum to the set temperature while monitoring the resistance and were allowed to stabilize at the chosen temperature. The saturation process itself took about 30 to 45 min. Then the samples were exposed to a pre-determined concentration of N_2O diluted with N_2 and the change in the resistance was monitored. At the saturation point of the adsorption, the gas flow was stopped and the experiment chamber was evacuated to allow the resistance to recover its original value. Table 1 compares the results obtained from the sensor experiments at different temperatures for both types of sensor. Although the nanowire mat sensor showed some detectable response at temperatures

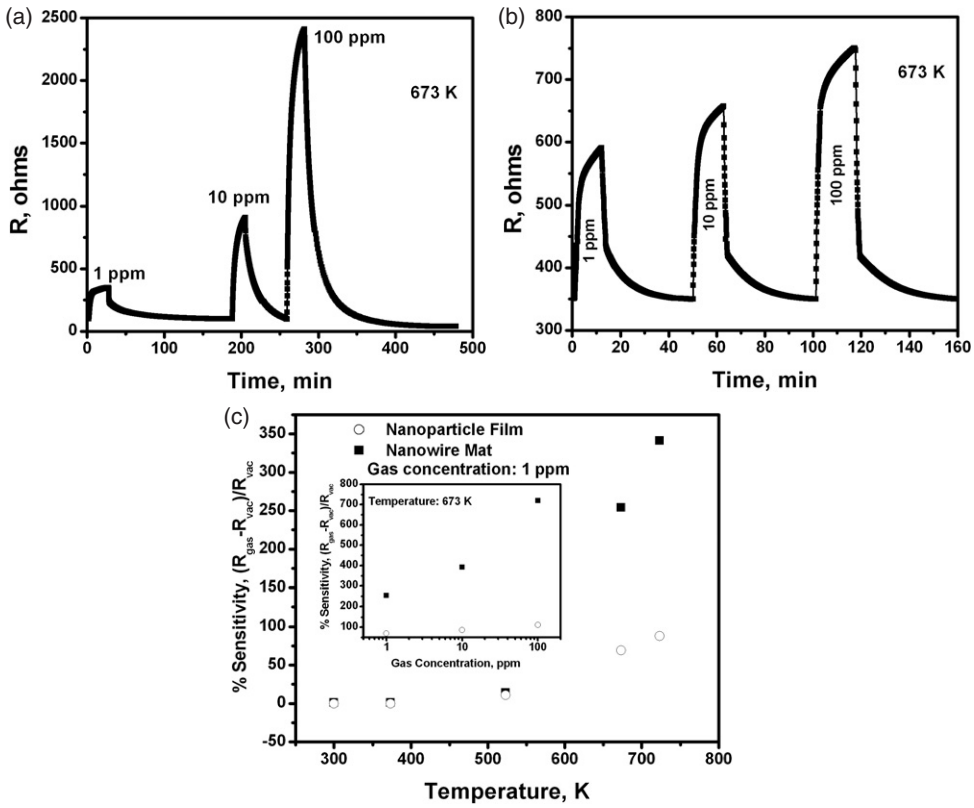

Figure 4. The electrical resistance response data with exposure to different gas concentrations for (a) nanowire mat and (b) nanoparticle thin films at 673 K. (c) The sensitivity of the nanowire mat is compared to that of nanoparticle thin films as a function of temperature at a 1 ppm concentration of N_2O. The inset shows the sensitivity as a function of gas concentration at 673 K.

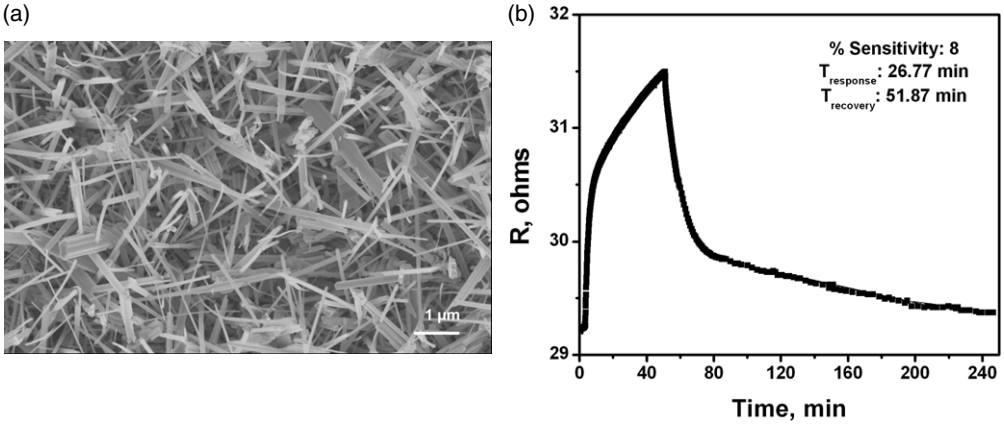

Figure 5. (a) Scanning electron micrograph of a randomly oriented nanowire sample and (b) typical sensor response of the nanowire film sample shown in figure 5(a) at 673 K and 1 ppm gas exposure.

Table 1. Comparison of gas sensing performance between nanowire mat and nanoparticle film samples at different temperatures.

Temperature (K)	Sensor type	Gas concentration (ppm)	Per cent sensitivity[a] $\frac{R_{gas}-R_{vac}}{R_{vac}} \times 100$	T90 response time (min)	T90 recovery time (min)
300	Nanowire mats	1	1	—	—
		10	3	—	—
		100	5	—	—
	Nanoparticle films	1	0	—	—
		10	0	—	—
		100	0	—	—
373	Nanowire mats	1	1	—	—
		10	2	—	—
		100	8	—	—
	Nanoparticle films	1	0	—	—
		10	0	—	—
		100	0	—	—
523	Nanowire mats	1	14	6.0	39.0
		10	38	28.0	36.5
		100	68	33.3	37.0
	Nanoparticle films	1	10.8	12.0	72.0
		10	12	31.0	51.2
		100	20	38.3	55.4
673	Nanowire mats	1	254	4.95	20.0
		10	393	10.5	37.0
		100	719	7.0	36.0
	Nanoparticle films	1	69	6.2	26.0
		10	86	11.4	38.0
		100	112	10.2	26.0
723	Nanowire mats	1	341	2.92	8.0
		10	2130	4.20	15.9
		100	2690	5.90	18.0
	Nanoparticle films	1	88	5.5	11.0
		10	144	5.63	10.4
		100	316	6.8	12.2

[a] R_{vac}: resistance measured at vacuum; R_{gas}: resistance of the sample after gas exposure.

below 523 K, the response and recovery time was quite high (∼3 h). The nanoparticle film sensor did not show any significant response at these temperatures. T90, the time required to reach 90% of the total change in resistance, response and recovery times were investigated for both types of sensor. For nanoparticle thin films, the recovery was slow and always led to overshooting. In order to get back to the base resistance, the operating temperature was always increased by 20–25° for a few minutes to obtain the response shown in figure 4(b).

Figure 4(c) clearly shows that higher sensitivity values were obtained with nanowire mats than with nanoparticle

Table 2. Parameters obtained from the fit of the nanowire sensor spectrum with equations (2) and (3). Time constants could be calculated from the first-order rate constant values.

Operating temperature (K)	Gas concentration (ppm)	Response zone $[\theta] = a - be^{-ct}$			Recovery zone $[\theta] = \theta_0 + \theta_1 e^{-ct}$		
		a	b	c	θ_0	θ_1	c
673	1	337	231	0.42	110	119.3	22.97
673	10	905	730	0.22	98	632	14.08
673	100	2374	2036	0.2	102	629.47	13.87
523	1	917	107	0.41	789	118.35	15.13
723	1	3720	2938.4	0.79	927	2444.4	6.18

films. The nanowire mats also exhibited much improved response and recovery times (see table 1). The lowest detectable concentration limit was estimated by extrapolating the sensitivity as a function of gas concentration to be about 100 ppb.

The sensing mechanism for N_2O involves the formation of electron accepting adsorbates on the surface of metal oxides as described elsewhere [31, 32]. The rate of increase in the electrical resistance in the response spectrum should be proportional to the steady state adsorbate concentration on the surface which could be estimated through a balance equation involving first-order kinetics of adsorption and desorption.

$$\frac{d[\theta]}{dt} = K_a[C] - K_d[\theta] \tag{1}$$

where K_a and K_d are adsorption and desorption rate constants respectively. The above equation can be solved for a given gas phase concentration, $[C]$, for steady state adsorbate coverage, $[\theta]$.

$$[\theta] = a - be^{-ct} \tag{2}$$

where a, b and c are constants that depend on the adsorption and desorption rates. The constant, a, is proportional to the adsorption rate and hence is directly proportional to the gas phase concentration. The constant, c, represents the rate constant involved with desorption and hence the time constant in the response curve. On the other hand, the rate of desorption would be dominant during recovery and the solution to equation (1) is of the form:

$$[\theta] = \theta_0 + \theta_1 e^{-ct} \tag{3}$$

where θ_0 and θ_1 are constants. The experimental response and recovery curves follow the trends given in equations (2) and (3). For networked nanowire sensors the response and recovery time constants were found to be 75 s and 6 min respectively at 723 K. Estimated rate constants of the nanowire sensor for different operating conditions are listed in table 2. The activation energy calculated from the slope of the time constant–temperature plot was ~26 kcal mol^{-1} for the nanowire device.

In order to understand the differences between different types of nanowire thin films for gas sensing, we deposited randomly oriented nanowire thin film as shown in figure 5(a). The typical response using such a nanowire film shown in figure 5(a) for detection of N_2O gas is shown in figure 5(b). The results show that the sensitivity of such a randomly oriented film is lower compared to that of the interconnected networked nanowire thin films but is similar to or better than that of nanoparticle thin films. These results, with modest improvements in sensitivity when using thin films containing randomly oriented nanowires, are consistent with earlier observations [22, 33]. For example, the performance of sensors made using a randomly oriented WO_3 nanowire film is improved in terms of sensitivity compared to that made using sol–gel processed tungsten oxide thin film [33]. But, both types of sensor seem to be significantly less sensitive than the interconnected networked nanowire mats reported in the present work. The main difference is with the extent of networking and sintered joints between the nanowires throughout the film.

Single nanowire devices on the other hand are known for their high sensitivity and extremely fast response and recovery time. In such cases, the active nanowire sensor element can act as a resistive element whose resistance can be changed by the charge transfer process occurring at the surface or as a field-effect transistor whose properties can be monitored by varying the gate potential. Single and multiple In_2O_3 nanowire based transistors have been shown to detect ppb levels of NO_2 and NH_3 [23, 34]. Although the response timescales for single metal oxide nanowire sensors depend on active sensor materials—as low as 40 s was reported for CO detection with SnO_2 nanowires [35]—the desorption kinetics of these single nanowire devices were found to be similar to that reported here. The response times (as well as recovery times) of the nanowire mats could possibly be improved further by reducing the distance between the contacts to several microns making them behave similar to single nanowire based sensors.

While the DC measurement gives information on the global sensor response, the alternating current (AC) approach offers a powerful tool to examine the nature of conduction processes and the mechanism of gas/solid interactions. For an applied AC signal under appropriate conditions, individual contributions from both the grain and grain boundaries to the overall sensor's resistivity can be resolved. A simple equivalent circuit comprising an R–C network [36–40] can be used to analyse the data and is shown in figure 6(a) along with its Nyquist plot. The impedance of the considered circuit is given by

$$Z = R_g + \left[\frac{1}{1/R_{gb} + j\omega C_{gb}}\right] \tag{4}$$

where R_g is the grain resistance, R_{gb} is the grain boundary resistance and C_{gb} is the grain boundary capacitance. The DC impedance is given by $(R_g + R_{gb})$ and the intercept of the impedance curve at high frequencies with the real axis equals R_g. By fitting the experimental response with that

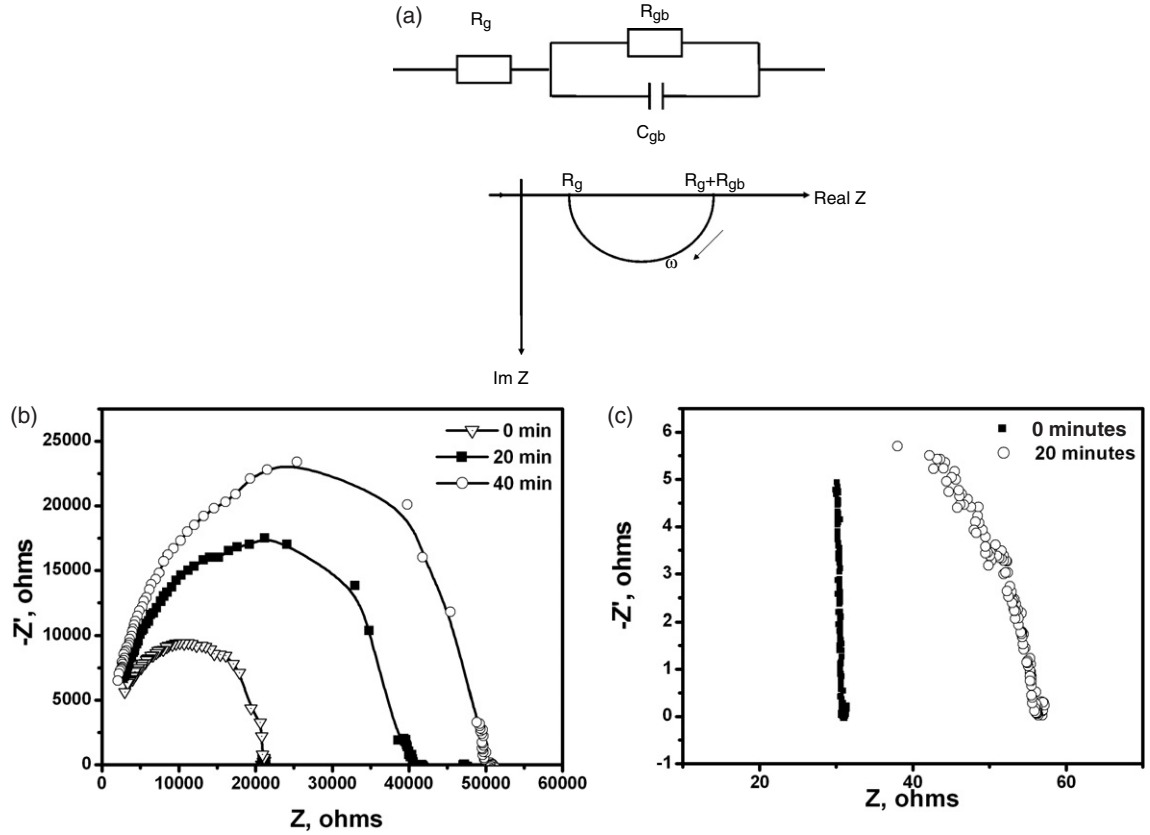

Figure 6. (a) The equivalent circuit model for analysing the impedance behaviour of thin film gas sensors. (b) The Nyquist plots of the impedance data obtained with the nanoparticle sensor before and after exposure at 673 K and (c) the Nyquist plots of the nanowire sensor before and after exposure at 673 K.

of the equivalent circuit, quantitative information about each contributing region can be obtained.

Figure 6(b) shows the transient response for the nanoparticle thin film sensor upon exposure to 10 ppm N_2O at 673 K. We constantly monitored the changes in the impedance spectrum with time after the introduction of gas species. The analysis of the data is presented in figure 6(b) for various contributions from grain resistance, grain boundary resistance and grain boundary capacitance. The grain boundary capacitance remains unchanged throughout the response period. The analysis shows that the grain resistance (R_g) does not vary considerably and the grain boundary resistance (R_{gb}) contributes mainly to the overall increase in the sensitivity. The impedance results with nanoparticle thin film sensors compare fairly well with the literature which established that the surface conductivity of a solid state metal oxide sensor is modified by adsorption of gas species and related space charge effects, and that the gas adsorption/desorption predominantly takes place at grain boundaries [37, 39, 41]. The sensitivity to the adsorbates at the grain boundaries also explains the slow timescales for recovery of sensing behaviour, i.e., the rate of desorption from grain boundaries is only equal to the ratio of grain boundary area to total surface area.

The transient impedance data were also obtained for nanowire mat samples as shown in figure 6(c). The analysis of the impedance data as summarized in table 3 clearly indicates that both grain resistance (in this case bulk nanowire resistance, R_g) and grain boundary resistance (certain nanowire/nanowire boundary resistance, R_{gb}) contribute significantly to the total resistance. These results indicate that highly networked nanowire thin film could behave similarly to a single nanowire or parallel nanowire array between two contacts as shown for SnO_2 nanowires by Kolmakov *et al* [35]. The results suggested that a sharp change in the bulk conductance of the nanowires occurs due to electron transfer from a surface state into the nanowires interior when it is exposed to trace gas. In our case, the results suggest that initially there exists a partially depleted state and that the conducting channel in the nanowires narrows or widens upon exposure to the oxidizing or reducing gas species.

Table 3. Change in grain and grain boundary resistance of the nanowire mats for exposure to different concentrations of gas. The data was obtained by performing semicircular fits on the corresponding Nyquist plots.

Gas concentration (ppm)	Gas exposure	R_g (Ω)	R_{gb} (Ω)	R_{total} (Ω)
1	Before	8.4	16.85	24.85
	After steady state	14.82	43.98	58.8
10	Before	9.7	20.93	30.63
	After steady state	69.51	167.59	237.1
100	Before	9.94	36.75	46.69
	After steady state	268	459	727

4. Conclusions

The highly networked nanowire mats are shown to be effective gas sensing materials with an order of magnitude higher sensitivity values compared to that of both the randomly oriented nanowires and nanoparticle films. The nanowire mat-like films have the potential to be integrated into sensors with few post-processing steps and also have the potential to achieve a performance closer to that of single nanowire devices. The impedance data showed that both grain boundary resistance and grain resistance change with exposure to gases for nanowire mats whereas only the grain boundary resistance changes for nanoparticle films.

Acknowledgment

The authors are grateful for financial support from the US Army Space Missile Defense Command W9113M-04-C-0024.

References

[1] Comini E 2006 *Anal. Chim. Acta* **568** 28
[2] Ionescu R, Hoel A, Granqvist C G, Llobet E and Heszler P 2005 *Sensors Actuators* B **104** 124
[3] Ionescu R, Hoel A, Granqvist C G, Llobet E and Heszler P 2005 *Sensors Actuators* B **104** 132
[4] Solis J L, Saukko S, Kish L, Granqvist C G and Lantto V 2001 *Thin Solid Films* **391** 255
[5] Tamaki J 2005 *Sensor Lett.* **3** 89
[6] Varghese O K and Grimes C A 2003 *J. Nanosci. Nanotechnol.* **3** 277
[7] Watson J 1984 *Sensors Actuators* **5** 29
[8] Yun M H, Myung N V, Vasquez R P, Lee C S, Menke E and Penner R M 2004 *Nano Lett.* **4** 419
[9] Tamaki J, Zhang Z, Fujimori K, Akiyama M, Harada T, Miura N and Yamazoe N 1994 *J. Electrochem. Soc.* **141** 2207
[10] Chung W Y, Sakai G, Shimanoe K, Miura N, Lee D D and Yamazoe N 1998 *Sensors Actuators* B **46** 139
[11] Khatko V, Gorokh G, Mozalev A, Solovei D, Llobet E, Vilanova X and Correig X 2006 *Sensors Actuators* B **118** 255
[12] Wang S H, Chou T C and Liu C C 2003 *Sensors Actuators* B **94** 343
[13] Chu X F, Wang C H, Jiang D L and Zheng C M 2004 *Chem. Phys. Lett.* **399** 461
[14] Fan Z Y and Lu J G 2005 *Appl. Phys. Lett.* **86** (12)
[15] Francioso L and Siciliano P 2006 *Nanotechnology* **17** 3761
[16] Heo Y W, Norton D P, Tien L C, Kwon Y, Kang B S, Ren F, Pearton S J and LaRoche J R 2004 *Mater. Sci. Eng.* R **47** 1
[17] Kalinin S V, Shin J, Jesse S, Geohegan D, Baddorf A P, Lilach Y, Moskovits M and Kolmakov A 2005 *J. Appl. Phys.* **98** (4)
[18] Kim I D, Rothschild A, Lee B H, Kim D Y, Jo S M and Tuller H L 2006 *Nano Lett.* **6** 2009
[19] Kolmakov A, Klenov D O, Lilach Y, Stemmer S and Moskovits M 2005 *Nano Lett.* **5** 667
[20] Patolsky F, Zheng G F and Lieber C M 2006 *Anal. Chem.* **78** 4260
[21] Wan Q, Li Q H, Chen Y J, Wang T H, He X L, Li J P and Lin C L 2004 *Appl. Phys. Lett.* **84** 3654
[22] Wan Q and Wang T H 2005 *Chem. Commun.* **30** 3841
[23] Zhang D J, Li C, Liu X L, Han S, Tang T and Zhou C W 2003 *Appl. Phys. Lett.* **83** 1845
[24] Kolmakov A and Moskovits M 2004 *Annu. Rev. Mater. Res.* **34** 151
[25] Xue X Y, Chen Y J, Wang Y G and Wang T H 2005 *Appl. Phys. Lett.* **86** (23)
[26] Shaw G, Parkin I P, Pratt K F E and Williams D E 2005 *J. Mater. Chem.* **15** 149
[27] Sysoev V V, Button B K, Wepsiec K, Dmitriev S and Kolmakov A 2006 *Nano Lett.* **6** 1584
[28] Ponzoni A, Comini E, Sberveglieri G, Zhou J, Deng S Z, Xu N S, Ding Y and Wang Z L 2006 *Appl. Phys. Lett.* **88** (20)
[29] Thangala J, Vaddiraju S, Bogale R, Thurman R, Powers T, Deb B and Sunkara M K 2007 *Small* **3** 890
[30] Salje E and Viswanathan K 1975 *Acta Crystallogr.* A **31** 356
[31] Kanazawa E, Sakai G, Shimanoe K, Kanmura Y, Teraoka Y, Miura N and Yamazoe N 2001 *Sensors Actuators* B **77** 72
[32] Kapteijn F, RodriguezMirasol J and Moulijn J A 1996 *Appl. Catal.* B **9** 25
[33] Sawicka K M, Prasad A K and Gouma P I 2005 *Sensor Lett.* **3** 31
[34] Zhang D J, Liu Z, Li C, Tang T, Liu X, Han S, Lei B and Zhou C 2004 *Nano Lett.* **4** 1919
[35] Kolmakov A, Zhang Y X, Cheng G S and Moskovits M 2003 *Adv. Mater.* **15** 997
[36] Daniel M F, Desbat B, Lassegues J C, Gerand B and Figlarz M 1987 *J. Solid State Chem.* **67** 235
[37] Labidi A, Jacolin C, Bendahan M, Abdelghani A, Guerin J, Aguir K and Maaref M 2005 *Sensors Actuators* B **106** 713
[38] Labidi A, Lambert-Mauriat C, Jacolin C, Bendahan M, Maaref M and Aguir K 2006 *Sensors Actuators* B **119** 374
[39] Ling Z, Leach C and Freer R 2002 *Sensors Actuators* B **87** 215
[40] Ling Z, Leach C and Freer R 2002 *Euro Ceramics Vii* Part 1–3 **206-2** 1465
[41] Kaur M, Gupta S K, Betty C A, Saxena V, Katti V R, Gadkari S C and Yakhmi J V 2005 *Sensors Actuators* B **107** 360